Vol. 3: 177–193, 1993 | CLIMATE RESEARCH Clim. Res. | Published December 30

The Köppen climate classification as a diagnostic tool for general circulation models

Ulrike Lohmann[1], Robert Sausen[2,4], Lennart Bengtsson[1], Ulrich Cubasch[3], Jan Perlwitz[3], Erich Roeckner[1]

[1]Max-Planck-Institut für Meteorologie, Bundesstraße 55, D-20146 Hamburg, Germany
[2]Deutsche Forschungsanstalt für Luft- und Raumfahrt (DLR), Institut für Physik der Atmosphäre, D-82234 Weßling, Germany
[3]Deutsches Klimarechenzentrum (DKRZ), Bundesstraße 55, D-20146 Hamburg, Germany
[4]Meteorologisches Institut der Universität Hamburg, Bundesstraße 55, D-20146 Hamburg, Germany

ABSTRACT: The Köppen climate classification was applied to the output of atmospheric general circulation models and coupled atmosphere-ocean circulation models. The classification was used to validate model control runs of the present climate and to analyse greenhouse gas warming simulations. The most prominent results of the global warming computations were a retreat of regions of permafrost and the increase of areas with tropical rainy climates and dry climates.

INTRODUCTION

For several decades atmospheric general circulation models (GCMs) and coupled atmosphere-ocean models have been used for studying climate and climate change. Usually, the models are verified by comparing certain model fields, such as temperature, pressure or wind, with the corresponding observations. Higher-order quantities, such as low- and high-frequency variability or the number of blocking events, have also been studied. The same quantities are usually also analysed in climate change simulations. In addition to these direct model variables, some combinations of variables are used which usually comprise long-time observational knowledge, e.g. the classification into 'Großwetterlagen' (Baur 1963). An additional approach is the classification that was introduced by Köppen (1923). Köppen divided the observed climates into several climate zones, such as 'Tropical Climate' or 'Polar Climate', using the annual cycles of near-surface temperature and precipitation. His classification also separates the zones in which different species of plants naturally grow.

Manabe & Holloway (1975) applied the Köppen classification to the Geophysical Fluid Dynamics Laboratory (GFDL) GCM. Since that time GCMs have been improved, both in resolution and physical parameterization, and it is worthwhile to apply Köppen's statistics to a state-of-the-art GCM. This method can also be applied in experiments to study how climate zones will shift in CO_2 warming simulations.

In the following sections we present Köppen's classification and apply it to observations. We then use the classification to validate the Hamburg atmosphere general circulation model ECHAM3, and we examine the shift of climate zones occurring in greenhouse gas warming simulations performed with the low resolution (T21) coupled atmosphere-ocean model ECHAM1/LSG and with the high resolution (T42) atmosphere model ECHAM3, which uses the sea surface temperature change simulated by the coupled model ECHAM1/LSG as input.

THE KÖPPEN CLIMATE CLASSIFICATION

In 1923 W. Köppen derived an effective classification of climate. Based on the idea that native vegetation is the best expression of climate, Köppen selected cli-

mate zone boundaries with the vegetation limits in mind; for example, the 10 °C isoline of the warmest month in the year is connected with the threshold of growing trees. Thus Köppen's classification is based on direct climate parameters: the annual cycles of temperature and precipitation.

Starting from monthly mean values, we denote the (long-term) annual mean near-surface (2 m) temperature by $\bar{t}$, and the monthly mean temperature of the warmest and coldest months by t_{max} and t_{min}, respectively. Correspondingly, $\bar{r}$ and r_{min} are the annual mean precipitation and the precipitation of the driest month. In addition, we define r_{smax}, r_{smin}, r_{wmax}, and r_{wmin} as the precipitation of the wettest summer month, the precipitation of the driest summer month, the precipitation of the wettest winter month and the precipitation of the driest winter month, respectively. Here the period from June to August is regarded as northern hemisphere summer and southern hemisphere winter. December to February are southern hemisphere summer and northern hemisphere winter. In defining the Köppen climate zones (types), temperatures are measured in °C, precipitation in cm per month (mo).

Köppen's classification makes use of a dryness threshold, r_d, which depends on the annual mean temperature and the annual cycle of precipitation:

$$r_d\ (\mathrm{cm\ mo^{-1}}) = \begin{cases} 2\bar{t}\ (^\circ\mathrm{C}) & \text{if at least 70\% of the annual precipitation occurs in winter;} \\ 2\bar{t}\ (^\circ\mathrm{C}) + 28 & \text{if at least 70\% of the annual precipitation occurs in summer;} \\ 2\bar{t}\ (^\circ\mathrm{C}) + 14 & \text{otherwise.} \end{cases}$$

Köppen distinguished 4 thermal climate types and 1 hydrological climate type. Each of the climate types is further subdivided into 2 or 3 subtypes. Definitions of the climate types and subtypes are given in Table 1. Examples of the different climates types and subtypes will be discussed in the following section.

We applied the Köppen classification to temperature data from Jones et al. (1991) and precipitation data from Legates & Willmott (1990). The Jones et al. data are monthly mean values of the sea-level temperature averaged over the period 1951 to 1980. For our purposes we determined the near-surface temperature using the mean orography and assuming a lapse rate of 0.65 K per 100 m. The precipitation data are based on observations from 1920 to 1980. However, data from recent years were more heavily weighted in the averaging procedure. Precipitation over the oceans was interpolated from coastal and island stations. Systematic errors were removed by regression analyses. South of 30° S, Legates & Willmott used the data of Jaeger (1976). The spatial resolution of data was reduced to the Gaussian grid used in a T21 spectral model (ca 5.6°).

Fig. 1 (upper panel) shows the climate zones determined from the data by Jones & Legates, hereafter referred to as J+L. Köppen's chart (Fig. 2) is well reproduced apart from the Dry Climates (type B), which extend far north of the Himalayas in Köppen's chart. The weak correspondence over the oceans with respect to the Dry Climates (B) and Humid Mesothermal Climates (C) between the 2 charts may be due to the lack of observations.

For illustration, the Jaeger (1976) precipitation data were also used to produce a climate zone chart (Fig. 1, lower panel; hereafter referred to as J+J). Fig. 3 (upper

Table 1. Climate classification of Köppen

Type Subtype	Description	Criterion
A	**Tropical Rainy Climates**	$t_{min} \geq 18\,^\circ\mathrm{C}$
Af	Tropical Rainforest Climate	$r_{min} \geq 6$ cm mo^{-1}
Aw	Tropical Savanna Climate	$r_{min} < 6$ cm mo^{-1}
B	**Dry Climates**	$\bar{r} \leq r_d$
BS	Steppe Climate	$\bar{r} \geq r_d/2$
BW	Desert Climate	$\bar{r} < r_d/2$
C	**Humid Mesothermal Climates**	$-3\,^\circ\mathrm{C} \leq t_{min} < +18\,^\circ\mathrm{C}$
Cs	Warm Climate with Dry Summer	$r_{wmax} \geq 3\,r_{smin}$
Cw	Warm Climate with Dry Winter	$r_{smax} \geq 10\,r_{wmin}$
Cf	Humid Temperate Climate	$r_{smax} < 10\,r_{wmin}$ and $r_{wmax} < 3\,r_{smin}$
D	**Humid Microthermal Climates**	$t_{min} < -3\,^\circ\mathrm{C}$ and $t_{max} \geq 10\,^\circ\mathrm{C}$
Dw	Cold Climate with Dry Winter	$r_{smax} \geq 10\,r_{wmin}$
Df	Cold Climate with Moist Winter	$r_{smax} < 10\,r_{wmin}$
E	**Polar Climates**	$t_{max} < 10\,^\circ\mathrm{C}$
ET	Tundra Climate	$0\,^\circ\mathrm{C} \leq t_{max} < +10\,^\circ\mathrm{C}$
EF	Permafrost Climate	$t_{max} < 0\,^\circ\mathrm{C}$

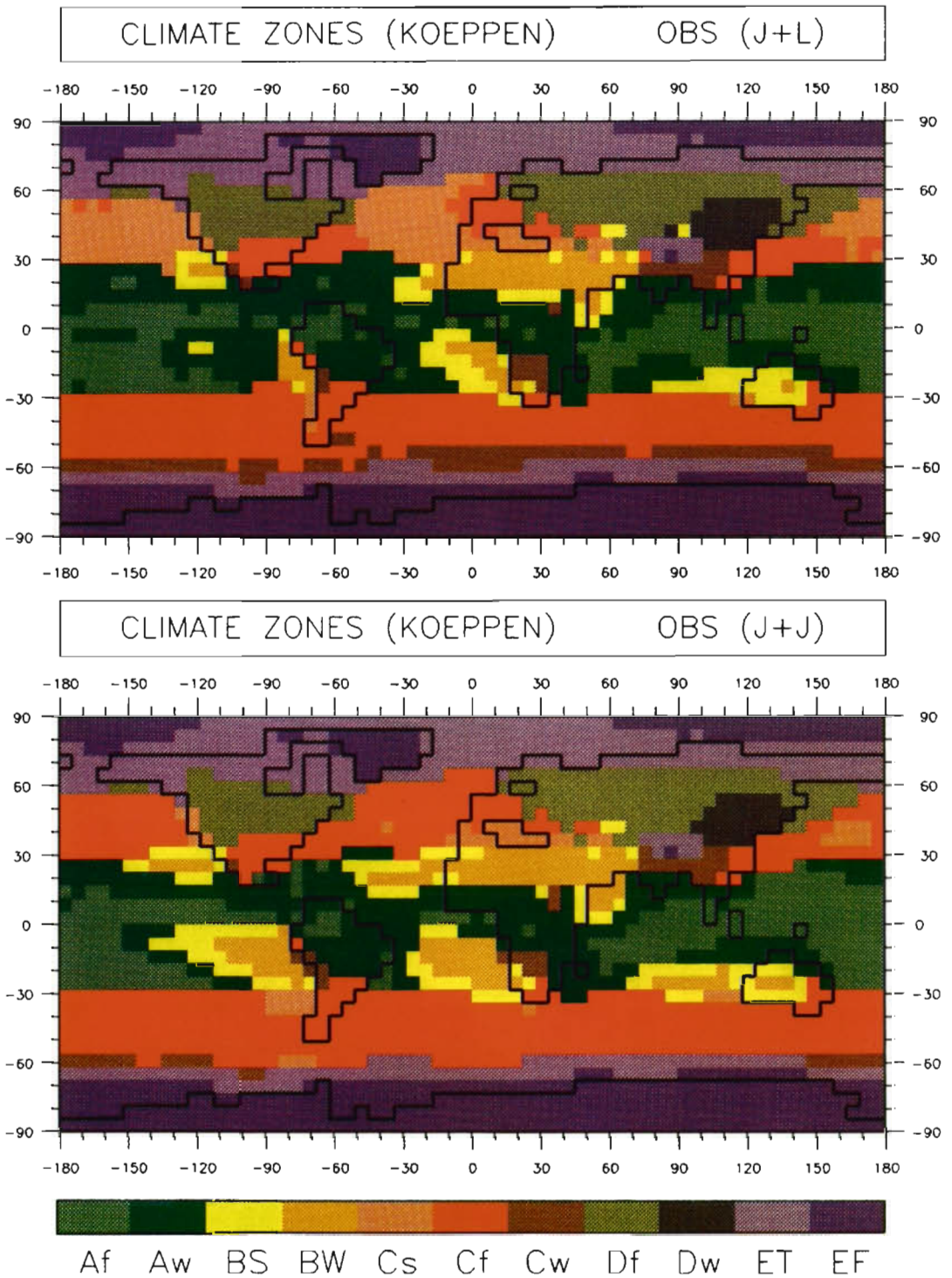

Fig. 1. Köppen climate zones based on observations of: (upper panel) Jones et al. (1991) and Legates & Willmott (1990); (lower panel) Jones et al. (1991) and Jaeger (1976)

panel) shows the fraction of the globe and of the continents covered by the different climate types and subtypes (see also Appendices 1 & 2). Compared to J+L, the Dry Climates (BW, BS) in J+J cover larger areas, especially over oceans, whereas less Tropical Savanna (Aw) is found in J+J. Another major difference is discernible in regions where J+J shows a Humid Temperate Climate (Cf) whereas J+L has a

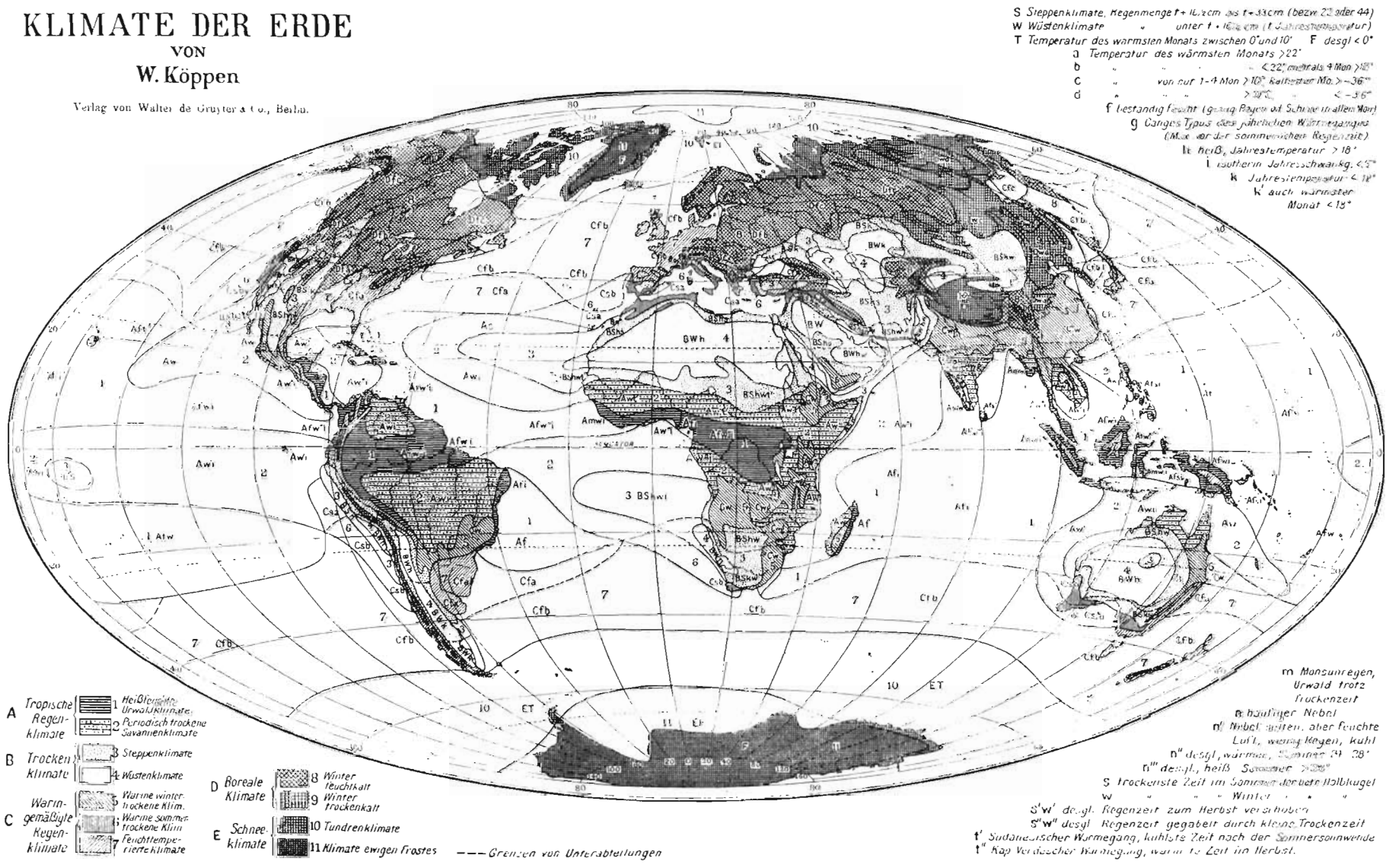

Fig. 2. Köppen's chart of climate zones (Köppen 1923). See Table 1 for definitions of classifications used in this study

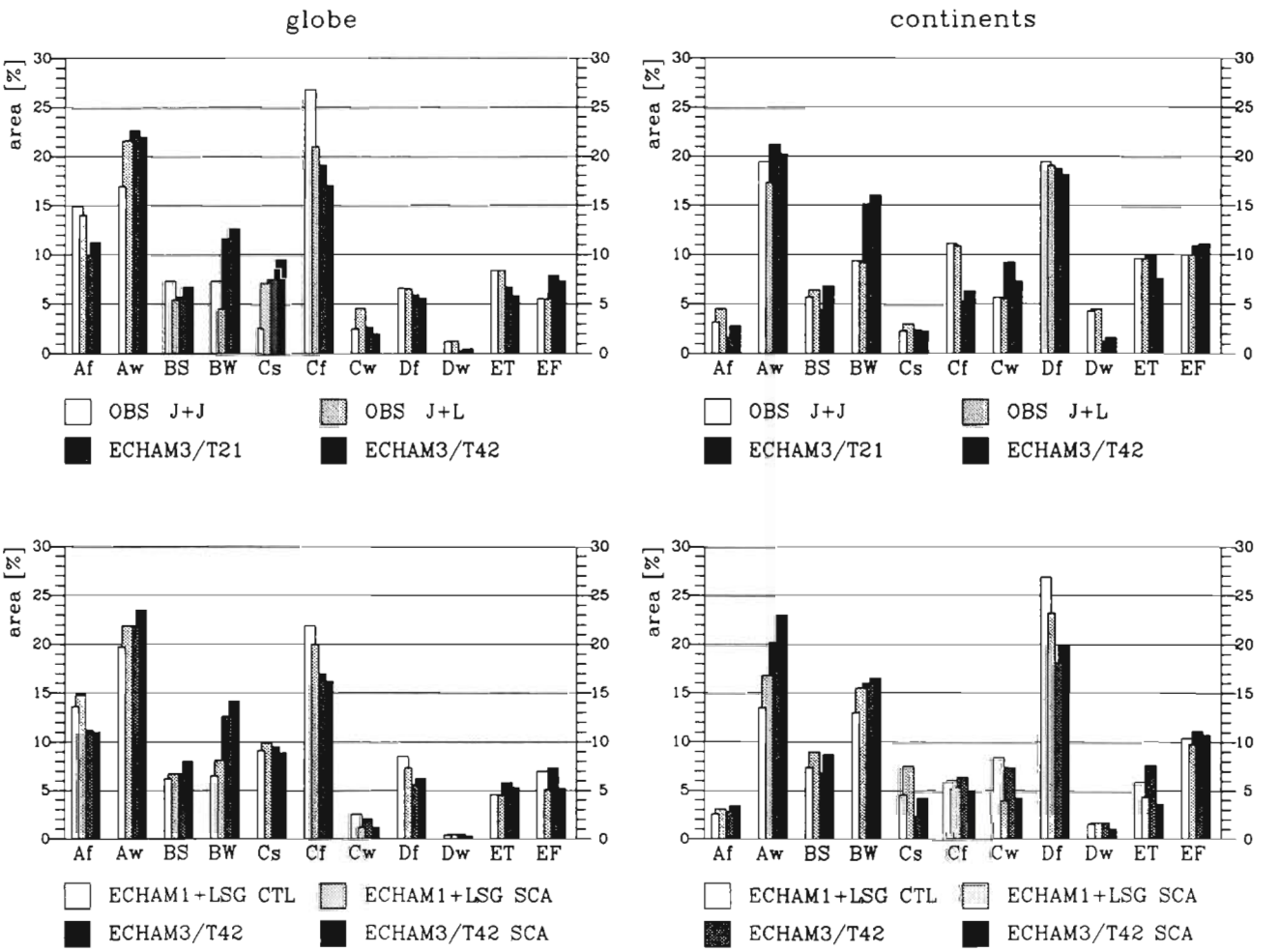

Fig. 3. Fraction of the globe (left panel) and of the continents (right panel) covered by different climate zones based on observations and model simulations. Upper panel: J+J, observations of Jones et al. (1991) and Jaeger (1976); J+L, observations of Jones et al. (1991) and Legates & Willmott (1990); S21, T21 uncoupled reference simulation with ECHAM3; S42, T42 uncoupled reference simulation with ECHAM3. Lower panel: CTL, T21 coupled control simulation with ECHAM1/LSG; SCA, T21 coupled Scenario A simulation with ECHAM1/LSG; S42, T42 uncoupled reference simulation with ECHAM3; A42, T42 uncoupled Scenario A simulation with ECHAM3

Mediterranean Climate (Cs), e.g. over the North Atlantic and North Pacific oceans. The differences between the 2 classifications are due to different precipitation data and indicate the uncertainties of the observations, which should be kept in mind when evaluating model climates.

SIMULATION OF CLIMATE ZONES WITH THE ATMOSPHERIC MODEL ECHAM3

Based on the numerical weather prediction model of the ECMWF (European Centre for Medium Range Weather Forecasts), the spectral general circulation model ECHAM was developed jointly by the Meteorologisches Institut der Universität Hamburg and the Max-Planck-Institut für Meteorologie, Hamburg, Germany. Prognostic variables are vorticity, divergence, temperature, (logarithm of) surface pressure, humidity and cloud water (solid and liquid phase). The model contains parameterizations of radiation, cloud formation and precipitation, convection, and vertical and horizontal diffusion. Land surface processes are described by a 5-layer heat conductivity soil model and by a hydrological model to determine evaporation and runoff. Currently the model is used mainly with 2 different horizontal resolutions, T21 and T42. The corresponding Gaussian grids for calculating the non-linear and the diabatic terms have a resolution of ca 5.6° and 2.8°, respectively. The model uses 19 vertical layers in a hybrid

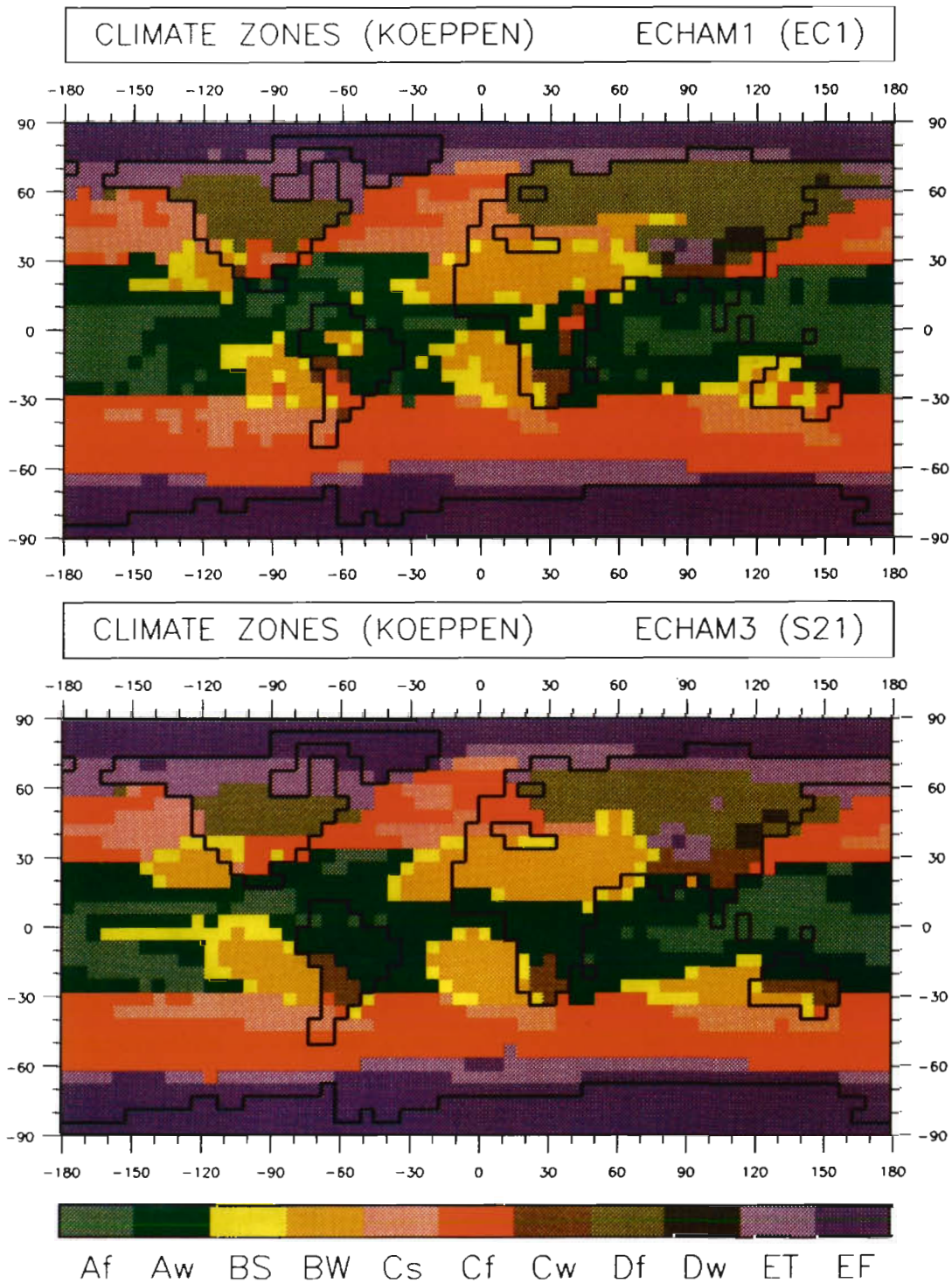

Fig. 4. Köppen climate zones as simulated by ECHAM1/T21 (upper panel) and by ECHAM3/T21 (lower panel) in reference runs with climatological sea surface temperature

σ-p-coordinate system. The annual and daily cycles of solar radiation are included. The annual cycle of sea surface temperature is given as the boundary condition. Currently 3 versions of the model exist (ECHAM1, ECHAM2, ECHAM3), representing successively more advanced versions. A comprehensive description can be found in Roeckner et al. (1992), which also contains a basic analysis of the model climate.

Here we examine 2 long-term integrations (30 yr) performed with ECHAM3 at resolutions T21 and T42

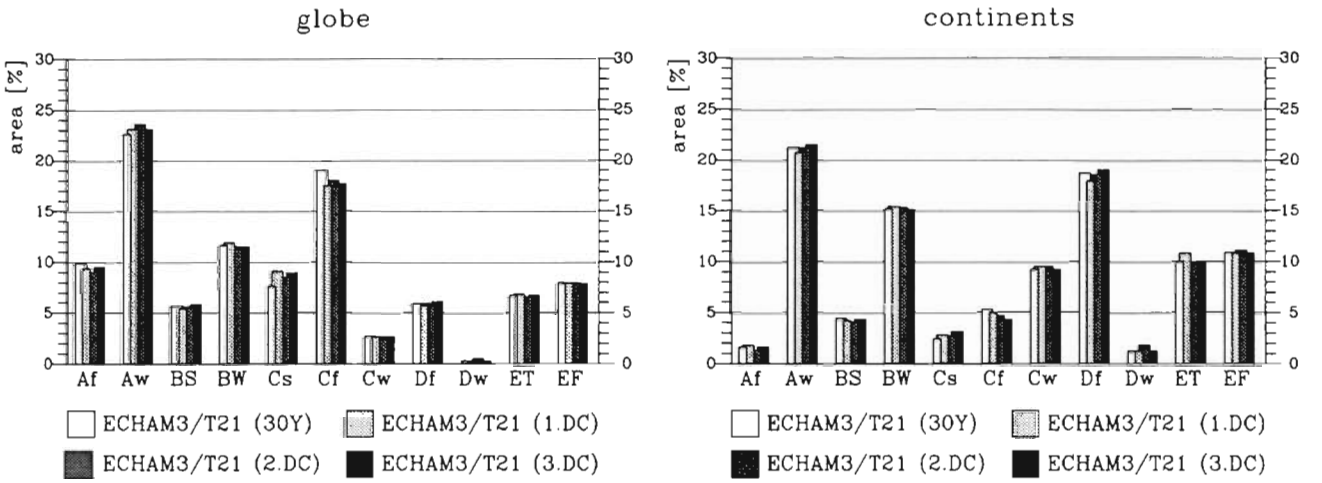

Fig. 5. As in Fig. 3 for the T21 uncoupled reference simulations using ECHAM3, with: 30Y, climate of the 30 yr period; 1.DC, climate of the first decade; 2.DC, climate of the second decade; 3.DC, climate of the third decade

respectively. For both runs the climatological sea surface temperature was used as the cyclo-stationary boundary condition (based on observations from 1979 to 1988). Fig. 4 (lower panel) shows the climate zones as simulated at the T21 resolution. The basic features of the observation-based distributions (Fig. 1) are reproduced, apart from the Dry Climates (BS, BW), which cover 17.3% of the globe in the simulation but only 9.9% in the observation of J+L (14.6% in J+J; see also Fig. 3). No Dry Climates show up north of the Himalayas (e.g. Gobi Desert). The Sahara Desert and Arabian Desert extend too far north. In contrast to the observed distribution, the model simulates Permafrost (EF) for the whole Arctic Ocean (except for the region north of Scandinavia and Russia). However, this is an artefact of the model, as sea ice of 2 m thickness without leads enters the model as a fixed parameter for the entire year.

In order to demonstrate the variability of the climate system we calculated the Köppen climate classification for each decade of the 30 yr control integration with ECHAM3/T21. The deviation of the climate zones from one decade to another is less than 1%, both for the globe and for continents only (Fig. 5). The climate zones of the 30 yr integration were calculated from the 30 yr monthly mean temperature and precipitation fields. The classification into Köppen climate zones is a nonlinear process. Therefore it cannot be expected that the area covered by a specific climate type in a long-term data set is the arithmetric mean of the areas covered by this climate type in each decade. For example, the distinctions within the Humid Mesothermal Climates (C) are derived from the relation of the driest or wettest summer month to the wettest or driest winter month. Since these extreme months can be different months, the averaging of temperature and precipitation before calculating climate zones can change the climate type. In the 30 yr mean a larger area of the globe is covered with Humid Temperate Climate (Cf) and a smaller area with Warm Climate with Dry Summer (Cs) than in each decade.

To illustrate the Köppen climate zones further, 12 grid points of the ECHAM3/T42 simulation were selected (Fig. 6) and their annual cycles of temperature and precipitation were plotted (Fig. 7). The indicated geographical longitudes and latitudes refer to the centre of the grid cell, and the name refers to a place located in the grid cell. Two grid boxes with Steppe Climate (BS) were selected, one representing a warm subtropical steppe [No. 3, Zinder (Niger)] and one representing a cold mid-latitude steppe [No. 4, Karaganda (Kazakhstan)].

These examples show that the climate of 'typical' model grid points appears similar to that which might be observed at a real climate station. However, as a single grid point is far below the dynamical resolution of a general circulation model, it is of no scientific value to compare these grid points with observations.

The shift of climate zones can be made more obvious if transfer matrices are considered (Table 2). The left part of Table 2 takes the whole surface of the globe into account, the right part only land points. The values represent the percentage of area that is of type *i* in J+L, but of type *j* in ECHAM3/T21, e.g. 4.7% of the area is of type A in J+L, but of type B in ECHAM3/T21. If the climates were identical in both realisations, values would occur only on the main diagonal. If the sum of the numbers above the main diagonal is larger than the sum of the numbers below, the second realisation (whose classes are listed horizontally, here S21) will have a 'colder' climate, i.e. an equatorward shifting of the climate zones.

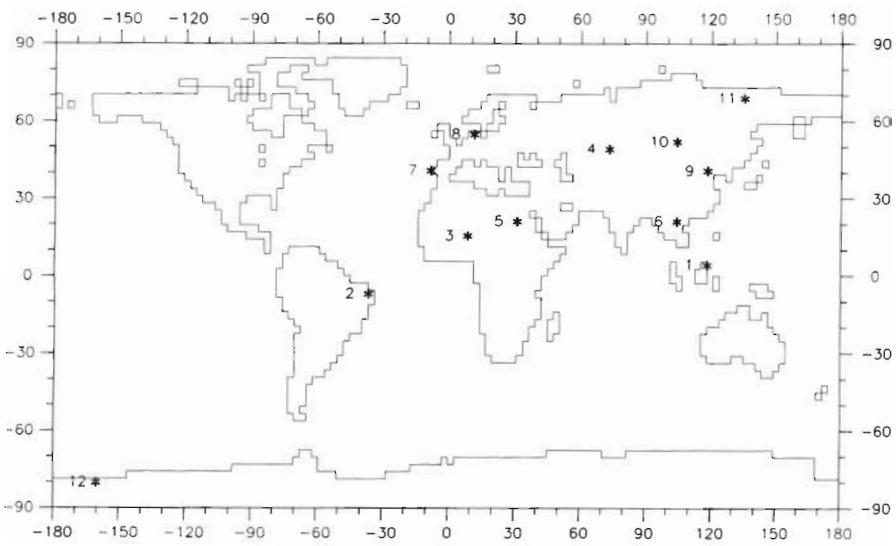

Fig. 6. Geographical positions of selected 'climate stations'

With regard to the large-scale pattern, the T42 simulation with ECHAM3 (Fig. 8, upper panel) is quite similar to the T21 reference simulation, but resolves more regional features. Examples of such features are the desert areas (BW) north of the Himalayas and the Tropical Rain Forest (Af) in Central Africa. But some model biases are also apparent, such as the desert extending too far south in East Africa, or the Cs climate in Western Europe occurring where Köppen (1923) shows Cf climate. However, these features are already below the dynamical resolution of the model (ca 480 km). Apart from such very small-scale features, the Köppen chart (1923) is reproduced reasonably well.

Since the Gaussian grids of the T21 and T42 resolutions do not coincide, we did not calculate the transfer matrices from observed climates or T21 model climates to the T42 model climate. Nevertheless, we can compare the fraction of the globe (continents) covered by a certain climate type or subtype (Fig. 3, upper panel) in these simulations. Obviously, the T42 simulation shows the largest fraction of B climates, in particular BW. On the other hand, C and D climates are underestimated.

SHIFTING OF CLIMATE ZONES IN GREENHOUSE GAS WARMING SIMULATIONS

In recent years the impact of anthropogenic changes in greenhouse gas concentrations has been studied using a variety of coupled atmosphere-ocean models. Cubasch et al. (1992) performed a series of four 100 yr simulations using the coupled atmosphere-ocean model ECHAM1/LSG. The atmospheric component of this model (at T21 horizontal resolution) differs from ECHAM3/T21 (described in the previous section) with respect to several aspects

Table 2. Transfer matrices from observations (J+L) to the uncoupled reference simulation with ECHAM3/T21 (S21). Values denote the percentage of the globe which is of type *i* in J+L but of type *j* in S21. Only values ≥0.1 are listed. The numbers at the bottom of the table are the sum of the matrix elements in the main diagonal (d) and above (a) and below (b) the main diagonal

Land and ocean

		S21 A	S21 B	S21 C	S21 D	S21 E
J+L	A	30.7	4.7	0.3		
	B	0.7	8.8	0.3	0.1	
	C	1.0	3.4	27.8	0.1	0.5
	D		0.5	0.3	6.2	0.8
	E			0.6	0.1	13.3

d = 86.7, a = 6.7, b = 6.6

Continental points only

		S21 A	S21 B	S21 C	S21 D	S21 E
J+L	A	20.3	0.5	1.0		
	B	1.0	13.5	1.2	0.2	
	C	1.5	4.0	14.0	0.2	
	D		1.6	0.5	19.5	1.5
	E			0.2		19.3

d = 86.6, a = 4.6, b = 8.8

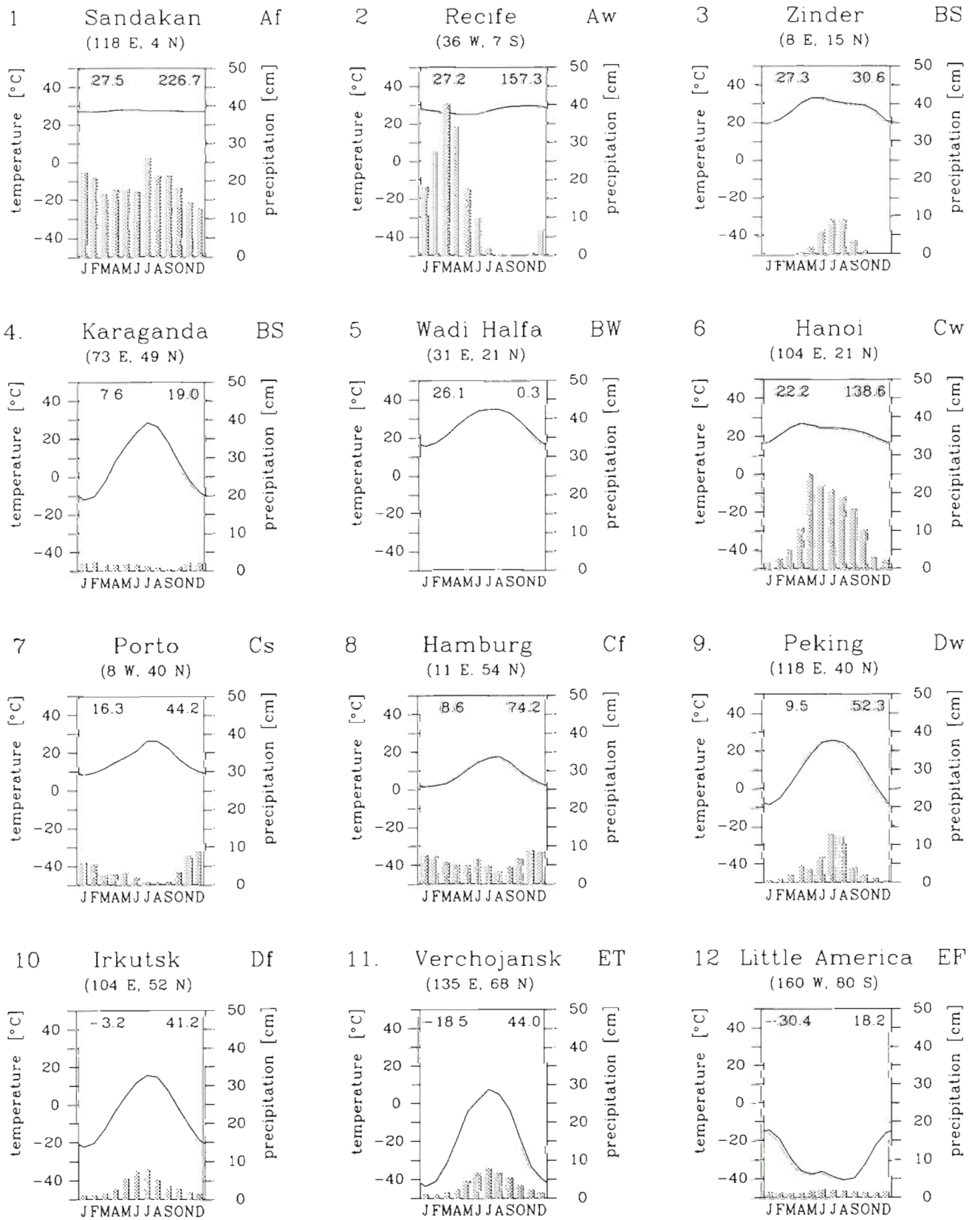

Fig. 7. Annual cycles of temperature and precipitation at selected grid points (see Fig. 6.) representing the different Köppen climate subtypes (from the T42 reference simulation with ECHAM3). Annual mean temperature (°C) is shown in the upper left corner of each chart, and annual precipitation (cm) in the upper right corner. The longitudes and latitudes refer to the centre of the grid cell, the name to a place located in the grid cell

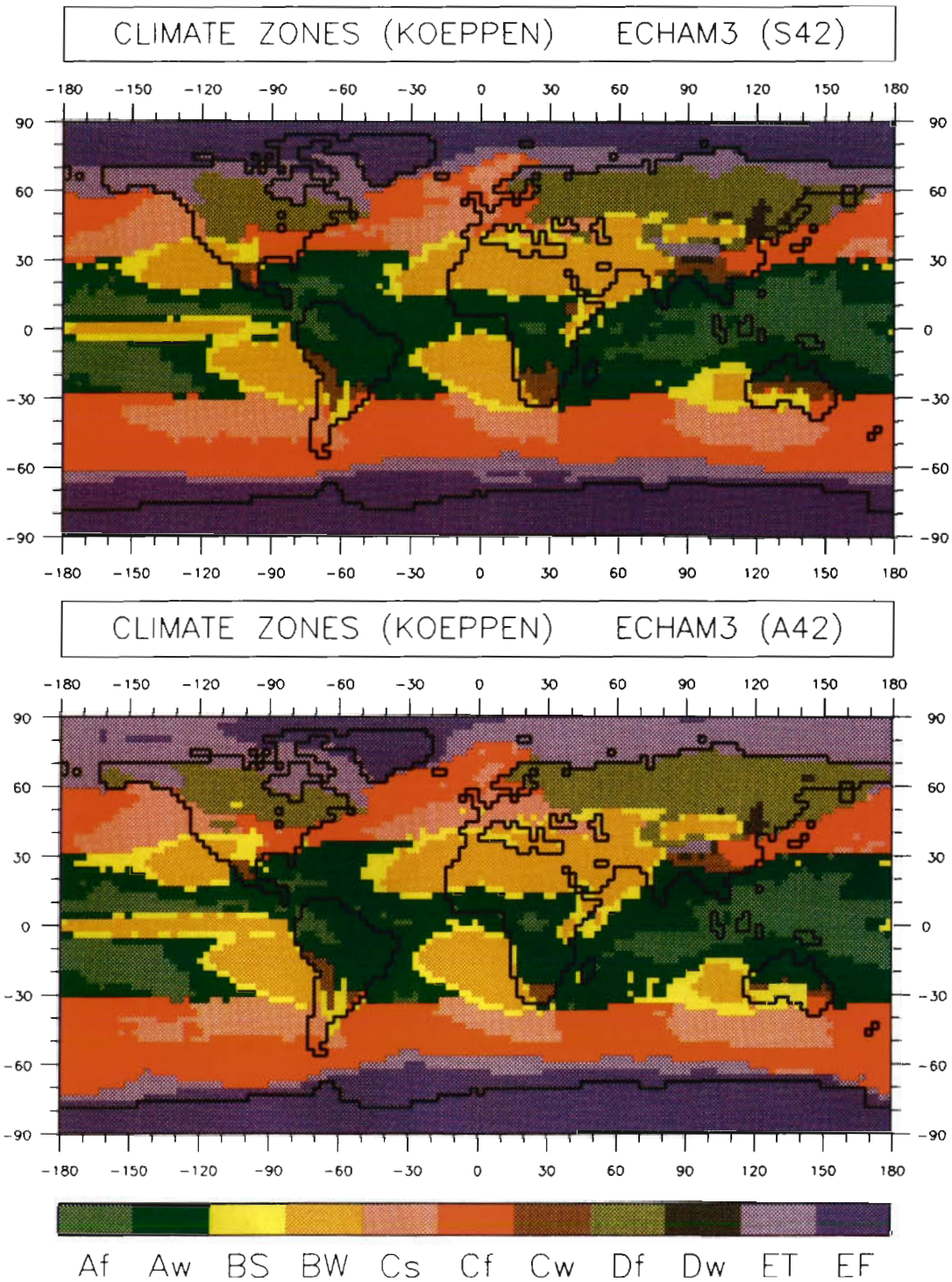

Fig. 8. Köppen climate zones as simulated by ECHAM3 (T42 horizontal resolution) in a reference run (upper panel) and in a Scenario A simulation (lower panel)

of the physical parameterizations. For example, as is described in Roeckner et al. (1992), ECHAM1 used the so-called Kuo convection scheme, as well as overly enhanced orographic forcing which included both the envelope orography and gravity wave drag.

The ocean model LSG is based on a numerical formulation of the primitive equations (Maier-Reimer &

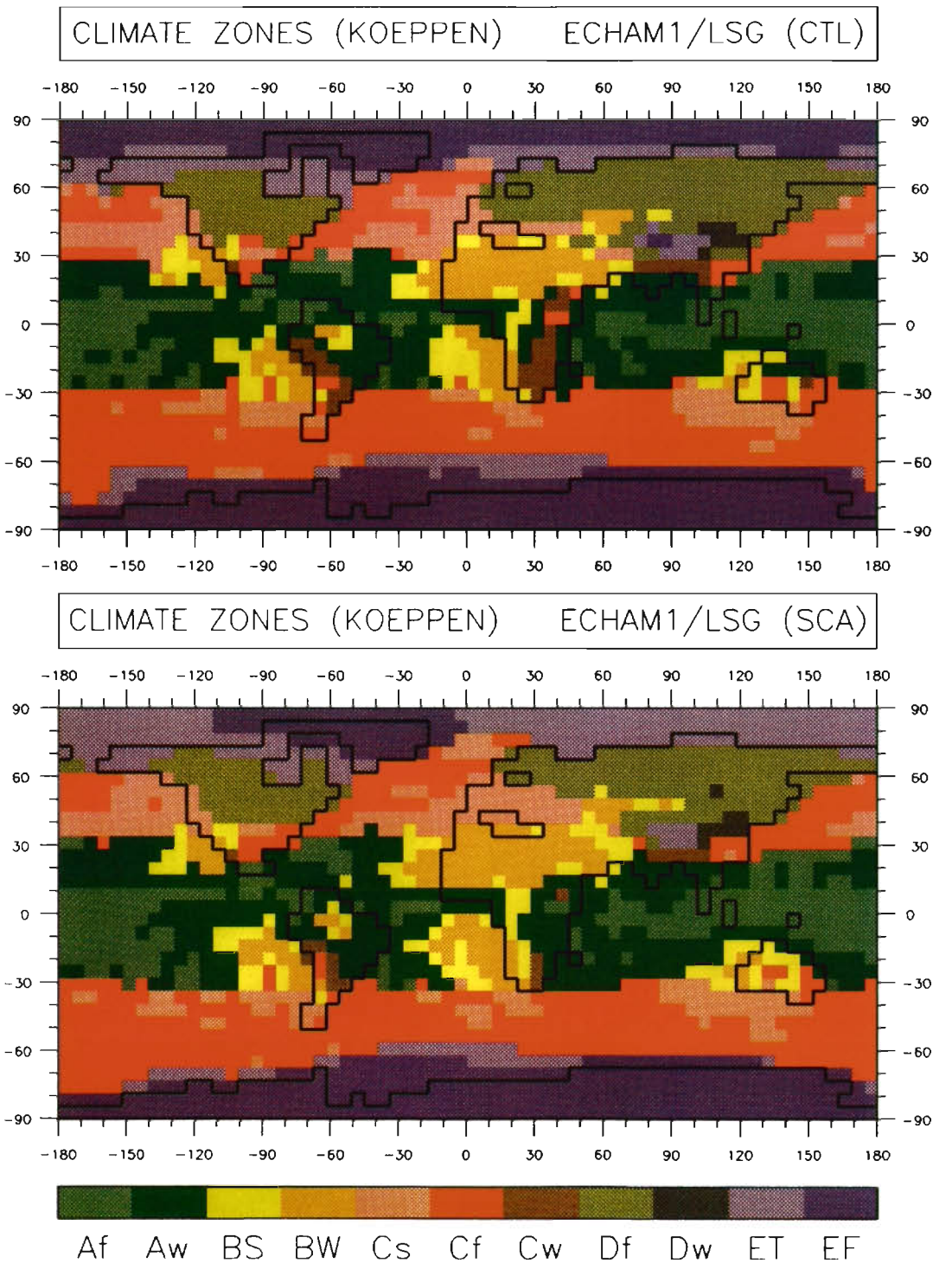

Fig. 9. Köppen climate zones as simulated by the coupled model ECHAM1/LSG for the control simulation (upper panel) and for the Scenario A experiment (lower panel)

Hasselmann 1987, Mikolajewicz & Maier-Reimer 1990) appropriate for Large-Scale Geostrophic motion. The non-linear advection of momentum is ignored and fast gravity waves are strongly damped by an implicit time integration scheme using a time step of 30 d. Salinity and temperature transports by currents are computed with an up-stream advection scheme. Vertical convective mixing is applied whenever the stratification be-

comes unstable. Sea-ice thickness is computed from the ice heat balance and advection by ocean currents, using a simplified viscous constitutive law. A realistic bottom topography is included.

The discretisation of the ocean model is based on 11 variably spaced vertical levels and 2 overlapping 5.6° × 5.6° horizontal E-grids (resulting in an effective grid size of 4°), which corresponds to the T21 Gaussian grid of ECHAM. In the coupled model simulations, the basic time step of 30 d is reduced to 1 d for the computation of the sea-ice thickness and the temperature and salinity in the 2 uppermost ocean levels, in order to resolve the more rapid response of the upper ocean to the short-term variability of the atmosphere.

The atmosphere and ocean components are coupled by the air-sea fluxes of momentum, energy (sensible and latent heat, shortwave and longwave radiation) and fresh water (precipitation minus evaporation plus river runoff along the coastal boundaries). The fluxes are calculated in ECHAM using the sea surface temperature and sea-ice thickness from LSG as surface boundary conditions. To avoid climate drift in the coupled system, a flux correction is applied (Sausen et al. 1988). Both models were integrated synchronously, but with their different time steps.

Four different CO_2 scenario simulations were conducted extending over 100 model years: control ('1×CO_2'), instantaneous doubling of CO_2 ('2×CO_2'), and IPCC Scenarios A and D (Houghton et al. 1990). In the control run the global mean of sea surface temperature was quite stationary, showing a decrease of less than 0.4 K during the 100 yr integration. In the 2×CO_2 experiment the temperature increased by 1.7 K in 100 yr. For Scenarios A and D the temperature rises were 2.6 and 0.6 K, respectively. More details of the experiments and their results can be found in Cubasch et al. (1992).

In the current paper we concentrate on the Köppen climate zones simulated in the last decade of the control and the Scenario A experiments. Fig. 3 (lower panel) shows the areal fraction of the globe (continents) covered by the individual climate types and subtypes. In Fig. 9 (upper panel) the Köppen climate zones for the control experiment (means for Years 91 to 100) are plotted. The main features of the (quite realistic) ECHAM3/T21 uncoupled reference simulation (Fig. 4, lower panel) are reproduced. A more detailed analysis, however, shows that the warmer climates are simulated less frequently, in particular Aw and BW (see also Appendices 1 & 2). This becomes more obvious if the transfer matrices are considered (Table 3).

However, this shift in climate zones can only partly be attributed to climate drift due to the coupling of the ocean and atmosphere models. The atmospheric component of the coupled model used an earlier version of ECHAM than that discussed in the previous section. Therefore, it is preferable to compare the coupled control integration with an uncoupled run performed with ECHAM1/T21. With this version a 20 yr reference integration was performed (20 identical cycles of sea surface temperature). Fig. 4 (upper panel) shows the Köppen climate zones for this run. Obviously the differences due to the coupling are now weaker. This is confirmed by the transfer matrices (Table 4; see also Appendices 1 & 2). A bias such as the desert occurring in the Amazon basin, which is also found in the ECHAM1 reference simulation, can be attributed to the severe truncation enhanced by the use of an envelope orography in ECHAM1 (caused by the Gibbs phenomenon).

Results of the Scenario A global warming experiment are shown in Fig. 9 (lower panel). The most prominent feature is a reduction of the Permafrost area (EF, from 7.0% to 5.1%). The Arctic Sea is free of ice. Consistent with the displacement of sea-ice, Tundra

Table 3. As in Table 2, but for the T21 uncoupled reference simulation with ECHAM3 (S21) and the T21 coupled control simulation with ECHAM1/LSG (CTL)

Land and ocean

		CTL				
		A	B	C	D	E
S21	A	29.7	1.3	1.5		
	B	3.6	10.9	2.4	0.4	
	C		0.3	28.1	0.9	0.1
	D		0.2	0.1	6.0	0.1
	E			1.4	1.7	11.5

d = 86.1, a = 6.6, b = 7.3

Continental points only

		CTL				
		A	B	C	D	E
S21	A	15.6	4.1	3.1		
	B	0.5	15.4	2.3	1.3	
	C		0.7	13.5	2.7	
	D		0.5		19.1	0.2
	E				4.9	16.0

d = 79.7, a = 13.7, b = 6.6

Table 4. As in Table 2, but for the T21 uncoupled reference simulation with ECHAM1 (EC1) and the T21 coupled control simulation with ECHAM1/LSG (CTL)

Land and ocean

		CTL				
		A	B	C	D	E
EC1	A	32.5	0.1	1.9		
	B	0.8	12.5	0.8	0.2	
	C		0.1	30.1	0.4	0.1
	D		0.1		8.2	0.2
	E			0.7	0.2	11.3

d = 94.6, a = 3.6, b = 1.8

Continental points only

		CTL				
		A	B	C	D	E
EC1	A	15.8	0.3	2.8		
	B	0.3	19.9	1.4	0.6	
	C			14.7	1.0	
	D		0.2		26.6	0.7
	E				0.2	15.5

d = 92.5, a = 6.8, b = 0.7

Climate (ET) in northern Siberia is replaced by Cold Climate with Moist Winter (Df). Another substantial change in climate is the increase in Tropical Rainy Climates (Af, from 33.3 % to 36.7 %), which can be seen in equatorial Africa and South America. The Dry Climates (B) also cover larger areas, increasing from 20.4 % to 24.5 % of the continental areas (see also Fig. 3). Fig. 10 identifies the grid points with a shift towards a colder climate (downward in Table 1) or to a warmer climate (upward in Table 1). Climate subtypes are not regarded. In 9.4 % and 0.9 % of the grid points, the Scenario A climate is of a 'warmer' and 'colder' type, respectively (see also Table 5).

Finally, we examined a Scenario A experiment (A42) performed with the uncoupled ECHAM3 model at T42 horizontal resolution (Perlwitz 1992). As a 100 yr simulation with ECHAM3/T42 would require more computational resources than presently available, the technique of time slicing was applied. First, the difference in the sea surface temperatures between Scenario A (mean of Years 91 to 100) and the control integration (mean of Years 1 to 10) was determined from the simulations with the coupled model ECHAM1/LSG. This difference was then added to the climatological sea surface temperature [as used in the ECHAM3/T42 reference simulation (S42) mentioned in the previous section]. Using the modified sea surface temperature and the mean CO_2 concentration for Years 91 to 100 (1045 ppm), a 30 yr integration was performed with the uncoupled atmosphere model ECHAM3/T42. This is a kind of 'stationary' Scenario A experiment. The global mean sea surface temperature is about 2 K higher on average then in the reference simulation (S42).

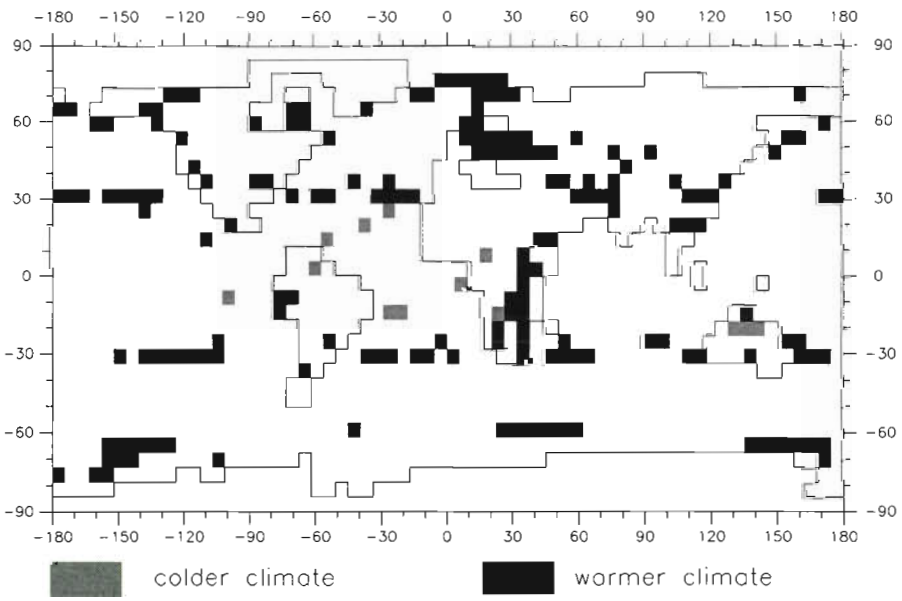

Fig. 10. Change of climate types from the control run to Scenario A as simulated by the coupled model ECHAM1/LSG

Table 5. As in Table 2, but for the T21 coupled control simulation and the T21 coupled ECHAM1/LSG (CTL) with Scenario A (SCA)

Land and ocean

		SCA				
		A	B	C	D	E
CTL	A	32.4	0.9			
	B	0.2	12.5			
	C	4.1	1.1	28.2		
	D		0.3	1.6	7.0	
	E			1.2	0.8	9.6

d = 89.7, a = 0.9, b = 9.4

Continental points only

		SCA				
		A	B	C	D	E
CTL	A	14.5	1.5			
	B	0.3	20.1			
	C	5.1	1.6	12.2		
	D		1.2	4.4	22.8	
	E				2.1	14.1

d = 83.8, a = 1.6, b = 14.6

Table 6. As in Table 2, but for the uncoupled ECHAM3/T42 simulation for the reference case (S42) and for the Scenario A case (A42)

Land and ocean

		A42				
		A	B	C	D	E
S42	A	31.3	1.8			
	B	0.3	18.9			
	C	2.9	1.2	24.3		0.1
	D		0.2	0.7	5.1	
	E			1.2	1.4	10.5

d = 90.0, a = 2.0, b = 8.0

Continental points only

		A42				
		A	B	C	D	E
S42	A	22.6	0.4			
	B	0.2	22.6	0.1		
	C	3.5	1.4	10.9		
	D		0.9	2.4	16.4	
	E			0.1	4.4	14.3

d = 86.8, a = 0.4, b = 12.8

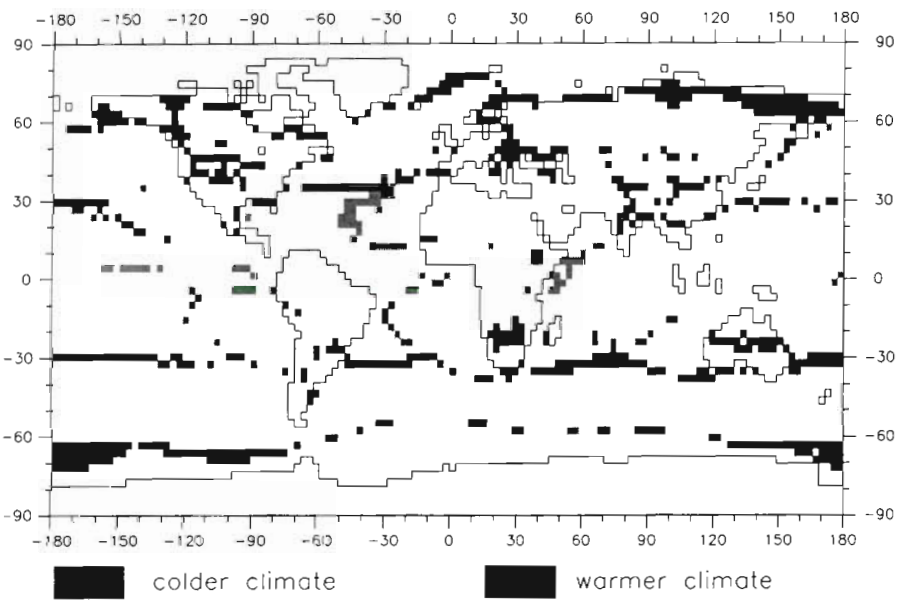

Fig. 11. As in Fig. 10, but for the uncoupled ECHAM3/T42 simulations

This Scenario A simulation (A42) allows the change in climate zones to be studied in more detail. Fig. 8 shows the Köppen climate zones for both the reference simulation (upper panel) and Scenario A (lower panel). As in the case of the T21 coupled ECHAM1/LSG simulations, there is a significant retreat of Permafrost Climate (EF), from 7.3% to 5.2% (see also Fig 3 and Appendices 1 & 2). Again an increase of Tropical Savanna Climate (Aw) is observed (from 21.9% to 23.5%), but the change is less pronounced than in the coupled simulations (CTL vs SCA). The Dry Climates (B), particularly the Desert Climate (BW), cover a larger area. The Humid Mesothermal Climates (C) show a general reduction. Humid Microthermal Climate (D) is expelled from Eastern Europe, although overall the D climates cover a larger area (e.g. in northeastern Siberia). The general shift towards warmer climates is also obvious from Table 6. Finally, Fig. 11 shows where changes in climate type occur. The Scenario A (A42) climate is of a warmer type in 12.8% of the continental area and of a colder type in only 0.4%.

In the IPCC report, Mitchell et al. (1990) selected 5 different climatic areas, for which they estimated the regional changes in temperature, precipitation and soil wetness in the year 2030 according to the 'business as usual' scenario from a simplified model, which was identical to the Scenario A used in our experiment. In each of these areas the temperature rose (by 1 to 4 K), but the precipitation changed in both directions. In central North America they estimated a warming of 2 to 4 K and increased precipitation of 0 to 15% in winter, whereas in summer the precipitation decreased by 5 to 10%. Consistent with these results, ECHAM3/T42 Scenario A shows more Humid Temperate Climate (Cf) instead of Cold Climate with Moist Winter (Df) in this region. In Southern Asia, A42 simulates Savanna (Aw), which replaces Warm Climate with Dry Winter (Cw). This is consistent with the increased summer precipitation (5 to 15%) and higher temperature (1 to 2 K) in Mitchell et al. (1990). The Dry Climates (B) extend far south of the Sahara in Scenario A, whereas in Mitchell et al. there is an increase in temperature (by 1 to 2 K) and precipitation in the Sahel zone. Since the Dry Climates are dependent on temperature and precipitation, a warmer climate with slightly increased precipitation could nevertheless remain a Dry Climate. For Southern Europe Mitchell et al. computed a warming of 2 K and increased precipitation in winter. During summer the temperature was also higher (2 to 3 K), but precipitation was reduced by 5 to 15%. Corresponding to this, A42 shows a shift from Warm Humid Climate (Cf) to Warm Climate with Dry Summer (Cs) in Central Europe and an expansion of Steppe (BS) far northwards into southwestern Europe. In Australia, A42 predicts extended Savanna regions (Aw), consistent with an increase in temperature by 1 to 2 K and precipitation by 10% as forecast by Mitchell et al.

An extension of the warmer climate zones towards the poles, and the regional changes mentioned above, can also be seen in the annual cycles of temperature and precipitation at the selected grid points of Fig. 7. At each point the temperature rises by 2 to 5 K, whereas the precipitation changes in both directions (Fig. 12). At 4 of the selected grid points the changes in the annual cycles of temperature and/or precipitation are large enough to result in a different climate zone.

CONCLUDING REMARKS

We applied the Köppen climate classification to a series of uncoupled and coupled simulations with the atmosphere general circulation model ECHAM. The uncoupled model ECHAM [especially the versions ECHAM2 (not shown) and ECHAM3] reproduces the observation-based classifications quite well. Even small-scale features such as the Gobi desert are reproduced in the ECHAM3/T42 reference simulation.

The control climate of the coupled model ECHAM1-LSG (T21) is somewhat too cold, especially in the tropics, relative to the uncoupled reference climate. The greenhouse gas warming computations with this model indicate a retreat of the Permafrost Climate (EF) and an extension of both the Tropical Rainy Climates (Af) and Dry Climates (B). This result also holds for the uncoupled ECHAM3/T42 simulations. However, the result for Humid Microthermal Climates (D) is of opposite sign in the coupled T21 and uncoupled T42 simulations, indicating the uncertainty of the model results.

An extension of the Köppen climate zones is the calculation of (stationary) biomes (Claussen & Esch 1992), which considers more model data relevant for biological systems. However, the Köppen classification is easier to apply and is still a useful tool for estimating the ability of climate models to reproduce the present climate as well as indicate the impact of climate changes on the biosphere.

Acknowledgements. This study was supported by the Bundesministerium für Forschung und Technologie (BMFT), grant 07 KFT 05/6, and the Commission of the European Communities under grant EPOCH-003-C(MB). We also thank Jörg Kaduk and Martin Heimann for providing us with the coloured graphics routines.

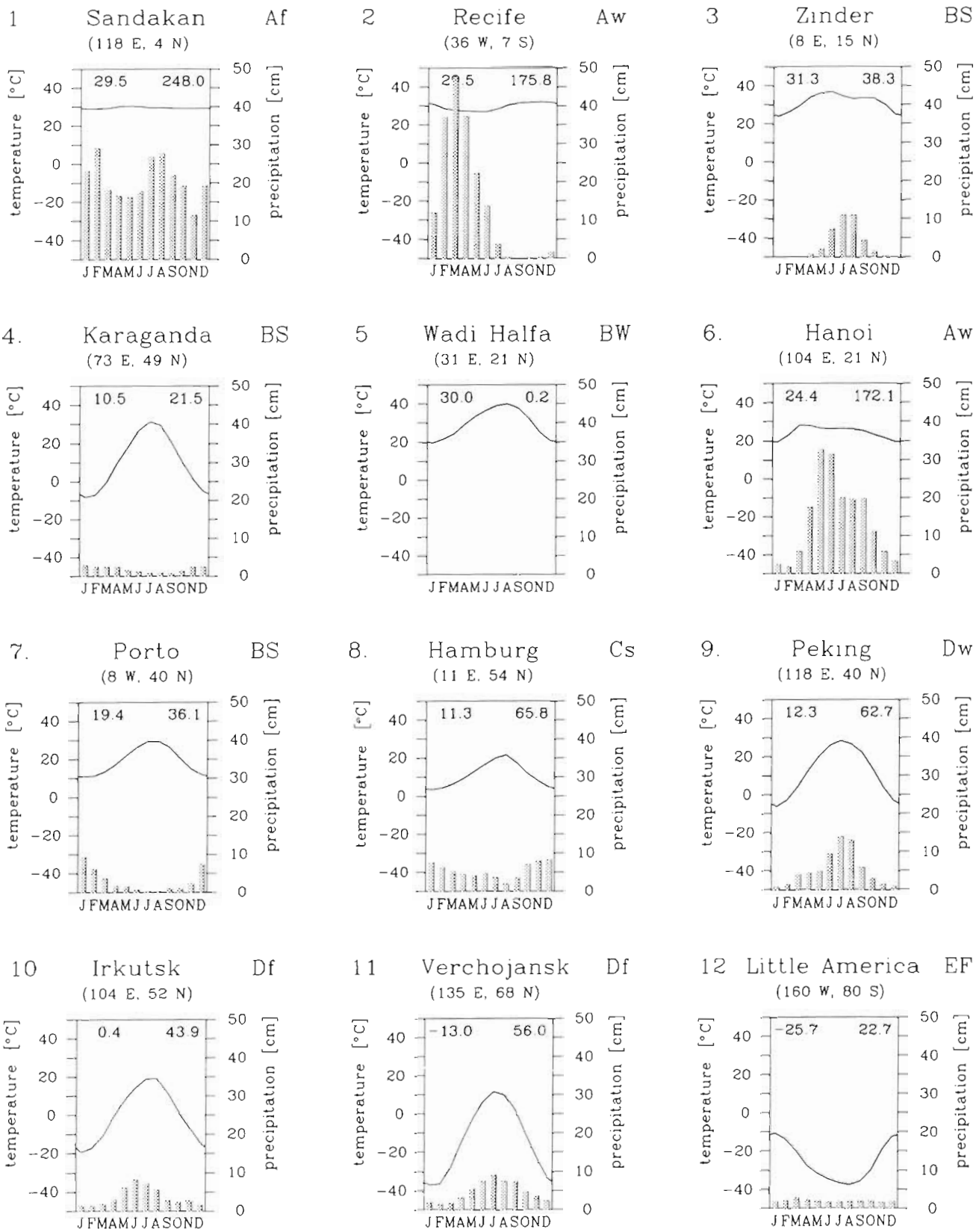

Fig. 12. As in Fig. 7, but for the uncoupled Scenario A simulation with ECHAM3/T42

LITERATURE CITED

Baur, F. (1936). Wetter, Witterung, Großwetter und Weltwetter. Z. angew. Met. 56: 377–381

Claussen, M., Esch, M. (1992). Biomes computed from simulated climatologies. Report No. 89, Max-Planck-Institut für Meteorologie, Hamburg

Cubasch, U., Hasselmann, K., Höck, H., Maier-Reimer, E., Mikolajewicz, U., Santer, B. D., Sausen, R. (1992). Time-dependent greenhouse warming computations with a coupled ocean-atmosphere model. Clim. Dyn. 8: 55–69

Houghton, J T., Jenkins, G. J., Ephraums, J J. (1990). Climate change. The IPCC scientific assessment. Cambridge University Press, Cambridge

Jaeger, L. (1976). Monatskarten des Niederschlags für die ganze Erde. Ber. Deutschen Wetterdienstes 139

Jones, P. D., Wigley, T M. L., Farmer, G. (1991). Marine and land temperature data sets: a comparison and a look at recent trends. In: Schlesinger, M. E. (ed.) Greenhouse-gas-induced climatic change: a critical appraisal of simulations and observations, Vol. 19. Elsevier, Amsterdam, p. 153–172

Köppen, W. (1923). Die Klimate der Erde. Walter de Gruyter, Berlin

Legates, D. R., Willmott, C. J. (1990). Mean seasonal and spatial variability in gauge-corrected, global precipitation. Int. J. Climatol. 10: 111–127

Maier-Reimer, E., Hasselmann, K. (1987). Transport and storage of CO_2 in the ocean – an inorganic ocean-circulation carbon cycle model. Clim. Dyn. 2: 63–90

Manabe, S., Holloway, J L. (1975). The seasonal variation of the hydrologic cycle as simulated by a global model of the atmosphere. J. geophys. Res. 80: 1617–1649

Mikolajewicz, U., Maier-Reimer, E. (1990). Internal secular variability in an ocean general circulation model. Clim. Dyn. 4: 145–156

Mitchell, J. F. B., Manabe, S., Tokioka, T., Meleshko, V. (1990). Equilibrium climate change and its implications in the future. In: Houghton, J. T., Jenkins, G. J., Ephraums, J. J. (eds.) Climate change. The IPCC scientific assessment. Cambridge University Press, Cambridge, p. 131–172

Perlwitz, J. (1992). Preliminary results of a global SST anomaly experiment with a T42 GCM. Ann. Geophys. Suppl. II to Vol. 10, C296

Roeckner, E., Arpe, K., Bengtsson, L., Brinkop, S., Dümenil, L., Esch, M., Kirk, E., Lunkeit, F., Ponater, M., Rockel, B., Sausen, R., Schlese, U., Schubert, S., Windelband, M. (1992). Simulation of the present-day climate with the ECHAM model: impact of model physics and resolution. Report No. 93, Max-Planck-Institut für Meteorologie, Hamburg

Sausen, R., Barthel K., Hasselmann, K. (1988). Coupled ocean-atmosphere models with flux correction. Clim. Dyn. 2: 154–163

Editor: G. Esser

Appendix 1. Fraction (%) of the globe covered by the different climate zones for observations and model simulations. J+J: observations based on Jones et al. (1991) and Jaeger (1976); J+L: observations based on Jones et al. (1991) and Legates & Willmott (1990); EC1: T21 uncoupled reference simulation with ECHAM1 (mean of 20 yr); S21 T21 uncoupled reference simulation with ECHAM3 (mean of 30 yr); S42: T42 uncoupled reference simulation with ECHAM3 (mean of 30 yr); CTL: T21 coupled control simulation with ECHAM1/LSG (mean of 10 yr); SCA: T21 coupled Scenario A simulation with ECHAM1/LSG (mean of 10 yr); A42: T42 uncoupled Scenario A simulation with ECHAM3 (mean of 30 yr)

Zone	J+J	J+L	EC1	S21	S42	CTL	SCA	A42
A	31.8	35.6	34.5	32.5	33.1	33.3	36.7	34.5
Af	14.9	14.0	13.2	9.9	11.2	13.6	14.8	11.0
Aw	16.9	21.6	21.3	22.6	21.9	19.7	21.9	23.5
B	14.6	9.9	14.3	17.3	19.3	12.7	14.8	22.2
BS	7.3	5.4	6.3	5.7	6.7	6.2	6.7	8.0
BW	7.3	4.5	8.0	11.6	12.6	6.5	8.1	14.2
C	31.9	32.8	30.7	29.4	28.5	33.5	31.1	26.3
Cs	2.6	7.2	9.4	7.6	9.5	9.1	9.9	8.9
Cf	26.8	21.0	19.8	19.1	17.0	21.9	20.0	16.2
Cw	2.5	4.6	1.5	2.7	2.0	2.5	1.2	1.2
D	7.8	7.8	8.5	6.2	6.1	8.9	7.8	6.5
Df	6.6	6.5	7.9	5.9	5.6	8.5	7.3	6.2
Dw	1.2	1.3	0.6	0.3	0.5	0.4	0.5	0.3
E	13.9	13.9	12.2	14.6	13.1	11.6	9.6	10.5
ET	8.4	8.4	5.4	6.7	5.8	4.6	4.5	5.3
EF	5.5	5.5	6.8	7.9	7.3	7.0	5.1	5.2

Appendix 2. As in Appendix 1, but only for continental areas

Zone	J+J	J+L	EC1	S21	S42	CTL	SCA	A42
A	22.6	21.8	18.9	22.8	23.0	16.1	19.9	26.4
Af	3.2	4.5	2.4	1.6	2.8	2.6	3.1	3.4
Aw	19.4	17.3	16.5	21.2	20.2	13.5	16.8	23.0
B	15.1	15.6	22.2	19.5	22.8	20.4	24.5	25.2
BS	5.7	6.4	7.8	4.4	6.8	7.4	9.0	8.7
BW	9.4	9.2	14.4	15.1	16.0	13.0	15.5	16.5
C	19.1	19.5	15.7	16.9	15.9	18.9	16.7	13.4
Cs	2.3	3.0	4.7	2.4	2.3	4.5	7.5	4.2
Cf	11.1	10.9	6.1	5.3	6.3	6.0	5.3	5.0
Cw	5.7	5.6	4.9	9.2	7.3	8.4	3.9	4.2
D	23.7	23.5	27.5	19.9	19.7	28.4	24.8	20.8
Df	19.4	19.0	25.5	18.7	18.1	26.9	23.2	19.8
Dw	4.3	4.5	2.0	1.2	1.6	1.5	1.6	1.0
E	19.6	19.6	15.7	20.9	18.7	16.2	14.1	14.3
ET	9.6	9.6	5.7	10.0	7.6	5.8	4.3	3.6
EF	10.0	10.0	10.0	10.9	11.1	10.4	9.8	10.7

Manuscript first received: October 9, 1992
Revised version accepted: July 1, 1993